Journal of Power Sources 195 (2010) 1308–1315

Contents lists available at ScienceDirect

Journal of Power Sources

journal homepage: www.elsevier.com/locate/jpowsour

Synthesis of nanocomposite nickel oxide/yttrium-stabilized zirconia (NiO/YSZ) powders for anodes of solid oxide fuel cells (SOFCs) via microwave-assisted complex-gel auto-combustion

Cai Tongxiang, Zeng Yanwei*, Zhang Wei, Guo Cuijing, Yang Xiaowei

State Key Laboratory of Materials-oriented Chemical Engineering, School of Materials Science and Engineering, Nanjing University of Technology, 5# New Model Road, Nanjing 210009, PR China

ARTICLE INFO

Article history:
Received 28 June 2009
Received in revised form
13 September 2009
Accepted 14 September 2009
Available online 20 September 2009

Keywords:
Auto-combustion synthesis
Nanocomposite powder
Nickel oxide–yttrium-stabilized zirconia
AC impedance
Temperature programmed reductions

ABSTRACT

Nanocomposite NiO/YSZ powders for high performance anodes of SOFCs have been synthesized via a microwave-assisted complex-gel auto-combustion approach using nitrates of Ni^{2+}, Zr^{4+} and Y^{3+}, citric acid (CA) and ethyl glycol as starting materials. The complexing conditions including pH and molar ratio of CA to the metal ions in the aqueous solutions have been quantitatively analyzed and optimized to realize their complete chelating into the CA-based gel network. The processing features and the microstructural characteristics of NiO/YSZ phases formed during auto-combustion of gels have been investigated by FT-IR, TG-DSC, XRD, SEM, SAED and HRTEM. It has been found that the nanoscale composite powders of NiO/YSZ, directly obtained through the *in situ* auto-combustion reactions within the gels, are composed of loosely agglomerated particles with sizes of ~200 nm, while these particles themselves are the aggregates of finer NiO and YSZ crystallites of ~15 nm in size. Moreover, the anodes prepared with such nanoscale composite powders have been manifested to possess much better electrochemical properties than the ones obtained by normal NiO/YSZ powder (~2.5 μm) according to their measurements of AC impedance and temperature programmed reduction behavior due to the highly enhanced three-dimensional transport network of oxide ions and triple-phase boundaries for surface reactions.

1. Introduction

Solid oxide fuel cells (SOFCs) can directly convert the chemical energy of fuels such as hydrogen, methane, methanol, etc. into electrical energy and are considered to be one of the most promising energy converters in the future [1–3]. Nickel/yttria stabilized zirconia ceramic–metal composite (Ni/YSZ cermet) is widely used as an anode material of SOFCs. It is commonly made from YSZ and NiO powders since the latter may be *in situ* reduced to metal nickel when exposed to fuel gas at working temperatures [4–5]. The Ni metal phase provides the pathway for electrons and catalytic activity for fuel gas to react at the surface of anodes, while the YSZ phase offers a conductance of oxide ions and creates interfacial sites with Ni particles for anodic reactions, apart from coordinating the thermal expansions of anode and electrolyte and suppressing the agglomeration and particle coarsening of Ni metal phase. Therefore, the anode electrochemical efficiency is closely associated not only with the intrinsic catalytic activities and transport properties of anode materials but with the particle morphology and composite microstructure of NiO and YSZ phases as well.

In recent years, considerable research efforts have been committed to the innovation of powder processing methods for better quality of anodes since the microstructural features of NiO–YSZ composites are found so strongly influenced by their synthesis processes [6]. NiO–YSZ composite powders are usually obtained by mixing NiO and YSZ powders. Nevertheless, the micro-sized powders cannot provide enough reactive sites for high performance anodes and often bring about the coarsening of Ni particles. On the other hand, although the nanosized powders are expected to establish plenty of reactive sites, they are frequently found very hard to reach a homogeneous mixing of NiO and YSZ particles mainly due to the easy agglomeration of ultrafine powders during processing. To solve these problems, Shao et al. [7], Shih et al. [8] and Mohebbi et al. [9] ever attempted to realize the synthesis and homogeneous mixing of nanosized NiO–YSZ powders by using sol–gel auto-combustion method.

In the present paper, a successful preparation of homogeneous nanocomposite NiO–YSZ powders by complex-gel microwave-assisted auto-combustion method is reported, together with the systematic studies of processing features and microstructural

* Corresponding author. Tel.: +86 25 83587254; fax: +86 25 83587254.
E-mail address: zengyanwei@tom.com (Z. Yanwei).

0378-7753/$ – see front matter © 2009 Elsevier B.V. All rights reserved.
doi:10.1016/j.jpowsour.2009.09.027

Table 1
The chelating reactions of CA with metal ions of Ni^{2+}, Y^{3+} and Zr^{4+} and their equilibrium constants.

No.	Main chelating reactions	Logarithm of reaction equilibrium constant
1	$C_6H_8O_7 = H^+ + C_6H_7O_7^-$	−3.10
2	$C_6H_7O_7^- = H^+ + C_6H_6O_7^{2-}$	−4.80
3	$C_6H_6O_7^{2-} = H^+ + C_6H_5O_7^{3-}$	−6.40
4	$Ni^{2+} + C_6H_7O_7^- = Ni(C_6H_7O_7)^+$	9.0
5	$Ni^{2+} + C_6H_6O_7^{2-} = Ni(C_6H_6O_7)$	4.8
6	$Ni^{2+} + C_6H_5O_7^{3-} = Ni(C_6H_5O_7)^-$	14.3
7	$Y^{3+} + C_6H_5O_7^{3-} = YC_6H_5O_7$	7.75
8	$Y^{3+} + C_6H_6O_7^{2-} = Y(C_6H_6O_7)^+$	4.55
9	$Y^{3+} + C_6H_7O_7^- = Y(C_6H_7O_7)^{2+}$	3.60
10	$Zr^{4+} + C_6H_5O_7^{3-} = Zr(C_6H_5O_7)^+$	8.00
11	$Zr^{4+} + 2C_6H_5O_7^{3-} = Zr(C_6H_5O_7)_2^{2-}$	14.00
12	$Zr^{4+} + C_6H_6O_7^{2-} = Zr(C_6H_6O_7)^{2+}$	10.80

characteristics of NiO–YSZ nanocomposite phases by FT-IR, TG-DSC, XRD, SEM, SAED and HRTEM techniques. In addition, the temperature-dependent AC impedance spectra and the temperature programmed reduction behavior of the anodes made of such nanocomposite powders were studied in comparison with the ones prepared by normal NiO/YSZ powder (~2.5 μm). It has been found that the nanosized NiO and YSZ crystallites tend to spontaneously aggregate into sub-micro composite particles, as the building blocks to constitute the powders when the complex-gel process and the auto-combustion of gels are well regulated. Furthermore, the nanocomposite NiO/YSZ anodes have been manifested to possess much better electrode properties than the normal ones according to their measurements of AC impedance and temperature programmed reduction behavior, probably arising from the highly enhanced three-dimensional oxide ion pathways and triple-phase boundaries. Therefore, it is believed that the nanoscale composite NiO/YSZ powders may greatly favor the performance enhancement of SOFCs' anodes.

2. Quantitative analysis of metal ions complexing by CA

In order to achieve the target nanocomposite NiO–YSZ powders, the metal ions Ni^{2+}, Zr^{4+} and Y^{3+} are expected to be chelated into the CA-based molecular network to form the homogeneous sols, which are subsequently converted into the gels with no segregations of the cations. Among the factors that may affect the sol formation and its stability, the pH value and the molar ratio of CA to metal ions (CA/M) in the solution are the important ones to remarkably influence the dissociation of citric acid and the formation of metal complexes. Therefore, the concentration variation of each metal-citrate species in the solution with pH and CA/M was theoretically calculated according to the equilibrium constants for the related chelations of CA with metal ions of nickel, yttrium and zirconium, which were outlined in Table 1 [10–13]. For the sake of simplicity, the trivial reactions of metal ions with NH_3 or OH^- were neglected in this study.

As the results of calculations, the variations of relative concentrations of metal ions in complexed species for nickel, yttrium and zirconium with respect to their total amounts are shown in Figs. 1–3, respectively, as a function of pH at the different CA/M ratios. It is clearly evident that the concentration sums of metal ions in complexed species generally increase as the pH value of solutions increases, except for the case of CA/M = 0.8, where a remarkable drop happens after the initial increase with the increasing of pH. Moreover, in this case, none of three metal ions can be chelated by CA to an extent larger than 99.9% over the whole range of pH. For the other CA/M ratios, the pH ranges, in which higher than 99.9% complexing of metallic ions for each kind with CA can be theoretically

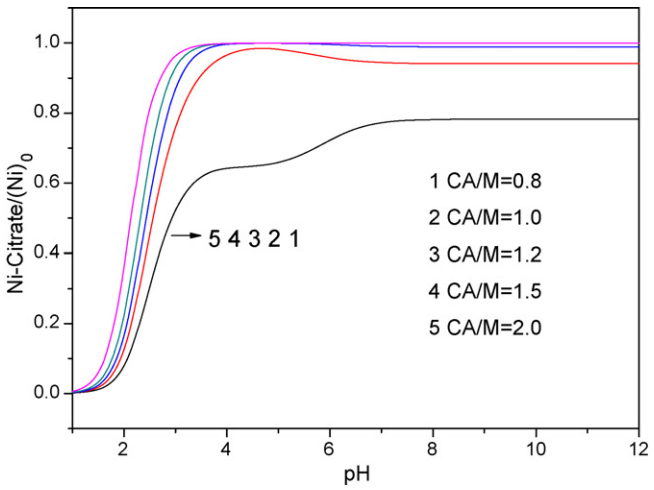

Fig. 1. The variation of Ni–citrates/$(Ni)_0$ as a function of pH at different CA/M, with $(Ni)_0$ denoting the total amount of Ni in the solution.

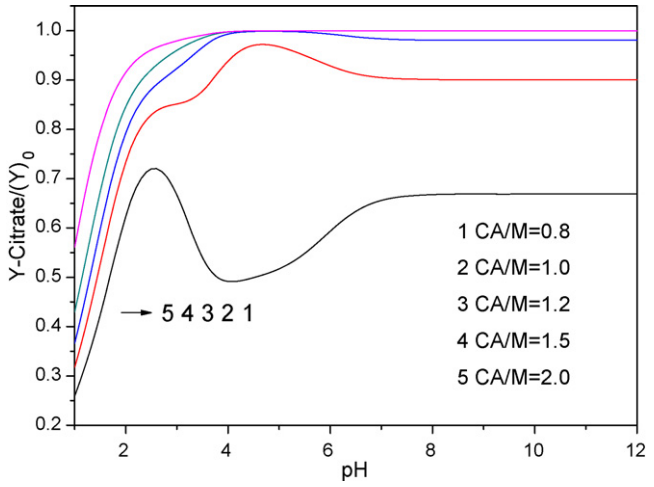

Fig. 2. The variation of Y–citrate/$(Y)_0$ as a function of pH at different CA/M, with $(Y)_0$ denoting the total amount of Y in the solution.

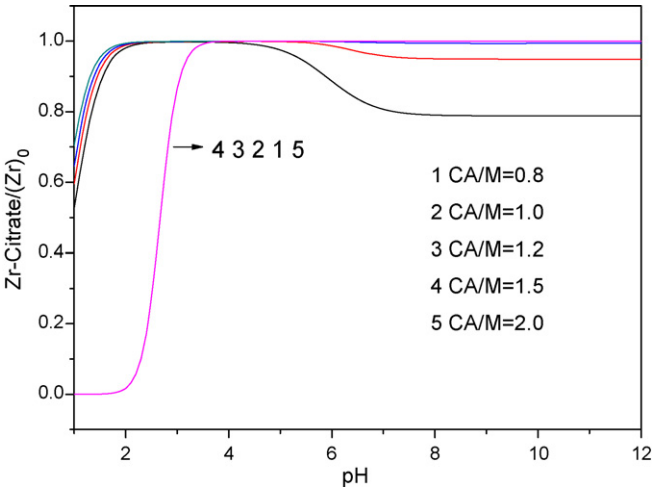

Fig. 3. The variation of Zr–citrate/$(Zr)_0$ as a function of pH at different CA/M, with $(Zr)_0$ denoting the total amount of Zr in the solution.

Table 2
The pH ranges for the metal–citrate concentrations > 99.9% at different CA/M.

CA/M	Ni–CA	Zr–CA	Y–CA
0.8	None	None	None
1.0	None	pH = 3–5	None
1.2	pH = 4.4–5.2	pH = 2.7–6.1	None
1.5	pH = 4.2–12	pH = 2.5–12	pH = 4.3–12
2.0	pH = 4.1–12	pH = 3.8–12	pH = 4.3–12

reached, were evaluated and presented in Table 2. These data can help determine the optimal chelating conditions to avoid the detrimental hydrations of metal ions. In the present study, CA/M = 1.5 and pH = 7 were selected as the optimal conditions to make all the metal ions entirely chelated by CA and, then, to transform into the homogeneous gels.

3. Experimental procedure

3.1. NiO–YSZ composite powder synthesis

In the present study, a weight ratio $W_{NiO}/W_{YSZ} = 1$ was chosen as the phase composition of NiO/YSZ composite powder, in which the YSZ phase was intended to contain 8 mol% Y_2O_3. The analytical grade nickel nitrate ($Ni(NO_3)_2{\cdot}6H_2O$), zirconium nitrate ($Zr(NO_3)_4{\cdot}5H_2O$), yttrium nitrate ($Y(NO_3)_3{\cdot}6H_2O$), citric acid ($C_6H_8O_7{\cdot}6H_2O$ or CA), ethylene glycol($C_2H_6O_2$ or EG), ammonium nitrate (NH_4NO_3) and NH_4OH were used as the starting materials. Firstly, stoichiometrical amounts of $Ni(NO_3)_2{\cdot}6H_2O$, $Zr(NO_3)_4{\cdot}5H_2O$ and $Y(NO_3)_3{\cdot}6H_2O$ were dissolved in an appropriate amount of deionised water together with CA and EG to form a aqueous solution, in which the molar ratios of CA to metal ions (CA/M) and EG to CA are 3/2 and 3/2, respectively. Then, aqueous ammonia of 28% was added dropwise into the solution until its pH reach 7. To make the auto-combustion of gels take place in a well-controlled manner and to ensure the formation of high quality NiO/YSZ powders, an appropriate amount of NH_4NO_3 was added into the solution to adjust the oxidation degree $Q = 0.8$, which is an index used to measure the extent to which the organics in the system would be oxidized by NO_3^- [14]. The solution was then continuously stirred at room temperature for 4 h for the formation of sol before it was heated at 80 °C for the removal of moisture to obtain the dried gel.

The auto-combustion of as-obtained gels was carried out in a microwave oven (1200 W, 2.45 GHz). The gels were compacted into pellets ($\phi 20 \times 5$ mm) and placed in a quartz glass beaker. They were ignited after about 10 s of microwave irradiation when the power output was set at 450 W and. Once on ignition, the combustion took place fiercely and lasted for about 15 s, resulting in a fluffy combustion product, which were then subjected to an annealing treatment in air at 600 °C and 800 °C for 2 h, respectively, to promote the formation of NiO–YSZ nanocomposites.

The whole preparation process is schematically illustrated in Fig. 4.

3.2. Process analysis and structural characterization

Thermogravimetry and Differential Scanning Calorimetry were adopted to probe thermochemical behavior of gels on a TG-DSC (Pyris 1 TGA, Diamond DSC) with a heating rate of 10 °C min^{-1} in N_2 to eliminate the influence from the surrounding air on the auto-combustion. For the phase identification and microstructural study, X-ray Diffractometer (ARL X'TRA) was used with Cu Kα radiation ($\lambda = 1.5406$ Å) and a tube power of 40 kV/35 mA. The infrared spectra (IR) to characterize the gels and the fluffy powders were recorded on an IR-FFT spectrophotometer (PE883) from 400 cm^{-1} to 4000 cm^{-1} by the KBr pellet method. A scanning electron microscope (SEM, JSM-5900) and a transmission electron microscope (HRTEM, JEM-2010 UHR) with select area electron diffraction (SAED) were also used to observe and characterize the microstructure of the NiO–YSZ composite particles.

3.3. Anode preparation and its property characterization

In order to relate the composite microstructures of nanosized NiO/YSZ crystallites to the anode's electrode performance, several discs with dimensions $\phi 20 \times 5$ mm were shaped with such nanocomposite powders at a pressure of 200 MPa by using starch as porosity controlling agent and then sintered at 1300 °C in air for 4 h. For comparison, the NiO and YSZ powders with an average size of ~2.5 μm were used to prepare the normal NiO/YSZ disc anodes with the same volume fractions for solid phases and pores as in the former. The sintered disc samples were carefully polished and coated with Ag-electrodes at the two end surfaces and the temperature-dependent AC impedance measurements (from

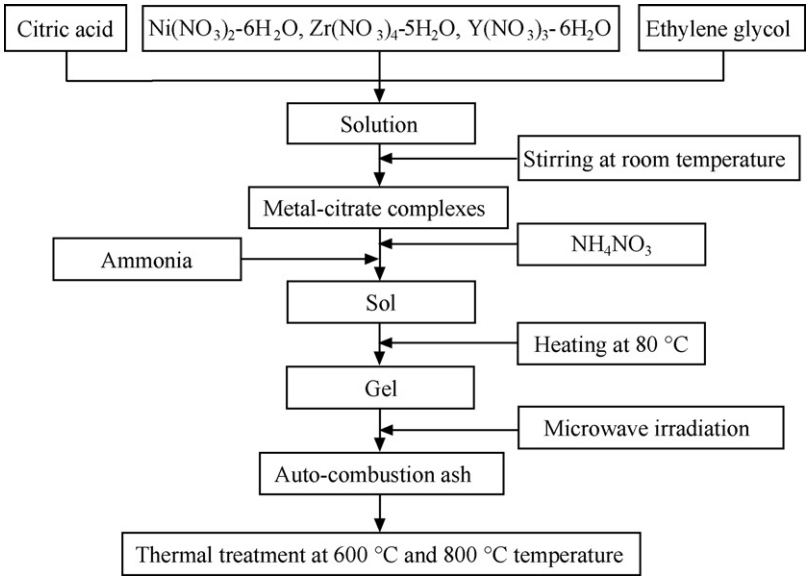

Fig. 4. Schematic diagram of the preparation of NiO–YSZ composite powders.

550 °C to 800 °C with an interval of 50 °C) were carried out on AC impedance spectroscopy (Solartron SI-1260) in the frequency range of 0.1 Hz to 1 MHz. For the temperature programmed reduction behavior measurement, the sintered samples were crushed into small pieces (~0.5 mm) and a Multifunctional Adsorption Instrument (AutoChem II 2920 model, Micromeritics, USA) was employed.

4. Results and discussion

Fig. 5 shows the typical IR spectra for the dried gels before auto-combustion and the auto-combustion product, as well as the pure citric acid for comparison. It can be seen that for the IR spectrum of dried gels (B), its major absorption bands appear at 1600–1660 cm^{-1} and at 1410–1380 cm^{-1} except for the ones in the high wavenumber region, which may be attributed to the asymmetric stretching vibrations and the symmetric ones of the carbonyls (COO^-) in the citrate carboxylate, respectively [15–17]. Moreover, these characteristic absorption bands can be found to have a shift to lower frequency compared with the ones of pure citric acid (A), corresponding to absorption bands at 1730 and 1427 cm^{-1} and suggesting that the vibration states of ligands have changed due to their chelation with metal ions [18]. Consequently, it is postulated that the metal ions such as Ni^{2+}, Y^{3+} and $Zr^{4+}$are all well chelated into the complexes. The peaks at 3134, 1767 and 1380 cm^{-1} are the typical bands of NH_4NO_3. It shows the presence of NO_3^- in the dried gel, which will act as oxidizing agent during the combustion [6]. In addition, the presence of absorption bands at 1081 and 1108 cm^{-1}, characteristic of the C–O groups [19], strongly suggests the formation of the organic network because of the polymerization and esterification of these complexes and EG molecules. Thereby, it is convinced that the metal ions are stochastically dispersed and located in the gel's network.

As regards the IR spectrum of the fluffy combustion product, the Curve (C) in Fig. 5 shows that the absorption bands at 1081 and 1108 cm^{-1} for C–O groups almost vanish and the bands at 1632 cm^{-1} and 1385 cm^{-1} corresponding to carboxyl groups are greatly reduced in comparison with the Curve (B) in despite of certain noticeable residuals. Obviously, it reveals the fact that the organics in the dried gel had been burned almost completely but there exist some unburnt substances because the oxidation index Q (0.8) was not large enough (~1.0). Nevertheless, there appears a new absorption band around 451 cm^{-1}, which may be assigned to (Ni, Zr)–O bond's stretching vibration mode

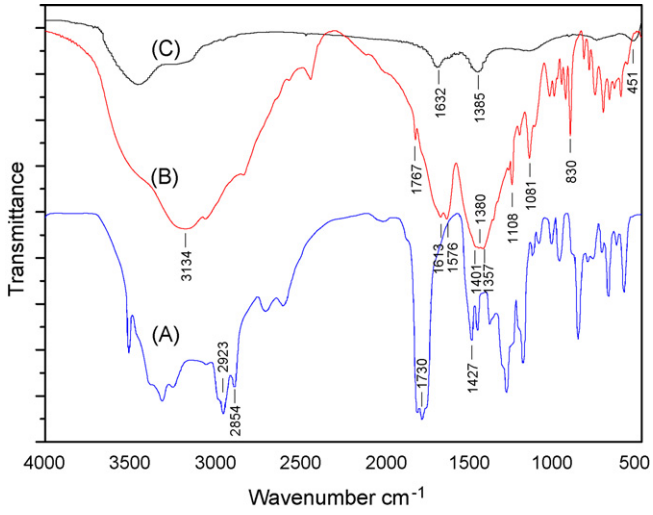

Fig. 5. FT-IR spectra of pure citric acid (A), dried gel (B) and combustion product (C).

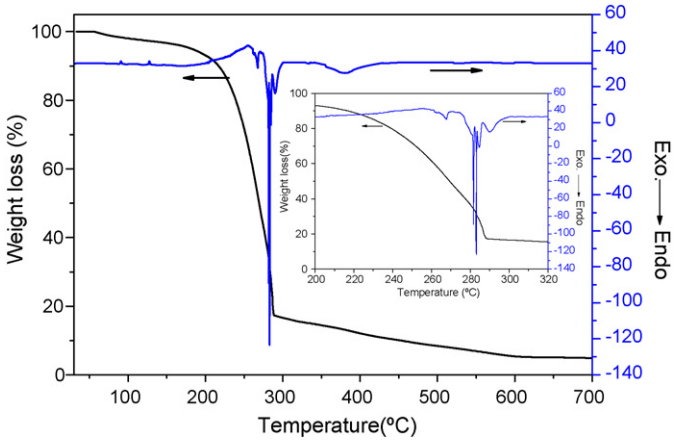

Fig. 6. DSC and TG curves of the dried gels obtained in N_2 atmosphere.

[20–21] and, therefore, implies the formation of oxides of Ni and Zr/Y.

Fig. 6 gives the typical DSC and TG curves for the gels that clearly exhibit a fiercely exothermic peak at 280 °C and a corresponding weight loss as much as 80%. These results suggest that the auto-combustion process is a bursting *in situ* redox reaction, in which CA and EG both act as fuels and NO_3^- ions do as an oxidant. However, it can be noted that the weight loss actually starts to happen as the temperature arrives around 60 °C and it seems to proceed at a constant speed before the temperature arrives at 170 °C. In the meantime, the DSC curve displays just a slight endothermal inclination. After that, the weight loss is increasingly accelerated until it reaches around 80% when the temperature comes at 280 °C, accompanied by a remarkable endothermal rise and then a small exothermal drop with DSC curve before the gigantic exothermal peak appears. Such a thermal behavior of the gels appears to indicate that a demoisture process may be involved from the room temperature to 170 °C, but the major decomposition of organics in the gels is supposed to happen before they are induced to begin burning fiercely at 280 °C and some species of decomposing products may be oxidized by fresh oxygen atoms released by NO_3^- at temperatures below 280 °C, referring to the presence of a small exothermal drop with the DSC curve. In addition, taking a closer look at the DSC curve in the neighborhood of 280 °C, the exothermic event is practically composed of 4 separate peaks that are respectively located at 278 °C, 283 °C, 285 °C and 290 °C, as shown in the inset with Fig. 6. The former two peaks are much intenser than the

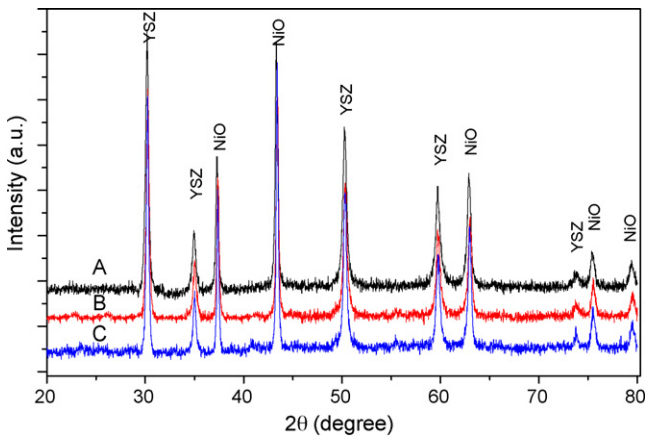

Fig. 7. XRD patterns for the samples of auto-combustion product (A) and the powders after the annealing at 600 °C (B) and at 800 °C (C) for 2 h.

latter two ones. It is believed that these exothermic peaks in the neighborhood of 280 °C result from the different burning behaviors of decomposing species of organics in the gels and are closely associated with the particular decomposing and *in situ* burning mechanisms of the organics.

However, no matter what details are involved in the burning process of the organics, the exothermic reactions all take place in a narrow temperature range around 280 °C. On the contrary, it really matters to reduce the time length for burn-booting because the longer time will bring about the escaping of more discomposing species in gas before the auto-combustion is ignited and then lead to no sufficient heat for the formation of target compounds. This is our consideration with which microwave energy is used to rapidly and uniformly heat the gels into burning.

Now let's turn to the microstructural characterization. Fig. 7 demonstrates the XRD patterns for the samples of auto-combustion product and the powders after an annealing treatment of the former at 600 °C and 800 °C for 2 h, respectively. It can be clearly seen that all three samples are composed of NiO and cubic YSZ phases and that no Ni metal phase can be found, compared with the cases of Mohebbi [9] and Marjanand [1]. This result may be ascribed to the incorporation of an appropriate amount of NH_4NO_3 in the gels and it guarantees the auto-combustions to proceed as it is expected to go. The crystallite sizes of NiO and YSZ phases in these three samples were estimated by Scherrer's equation and are shown in Table 3. It is interestingly found that the NiO and YSZ grains in the combustion product are as small as 14 nm in diameter and that they both show almost the same grain size regardless of their big difference in the crystallization behavior. It is believed that such a phenomenon of equal-size crystallites for NiO and YSZ phases in the combustion products may arise from the short-time *in situ* burning reactions in a highly homogeneous gel because the homogeneous distribution of metal ions and short-time auto-combustion greatly limit the long-range diffusion of reactants. Therefore, the relative sizes of their oxide crystallites are mainly determined by the local stoichiometric relation between the metal ions. Obviously, nearly the same sizes of NiO and YSZ crystallites in the combustion product are consistent with the fact that the samples have the same weights of NiO and YSZ, as aforementioned in Section 3.1. After annealing treatments at 600 °C or at 800 °C, the grain sizes of NiO and YSZ phases both show a slight increase and the former is relatively bigger than the latter, as shown in Table 3.

Table 3
XRD Scherrer's sizes of NiO and YSZ crystallites in the powder samples.

Phase	Combustion product	Annealed at 600 °C × 2 h	Annealed at 800 °C × 2 h
YSZ	14.2	14.3	15.6
NiO	14.7	15.1	18.2

As regards the microstrucural features of the auto-combustion products, the typical SEM image is illustrated in Fig. 8, along with

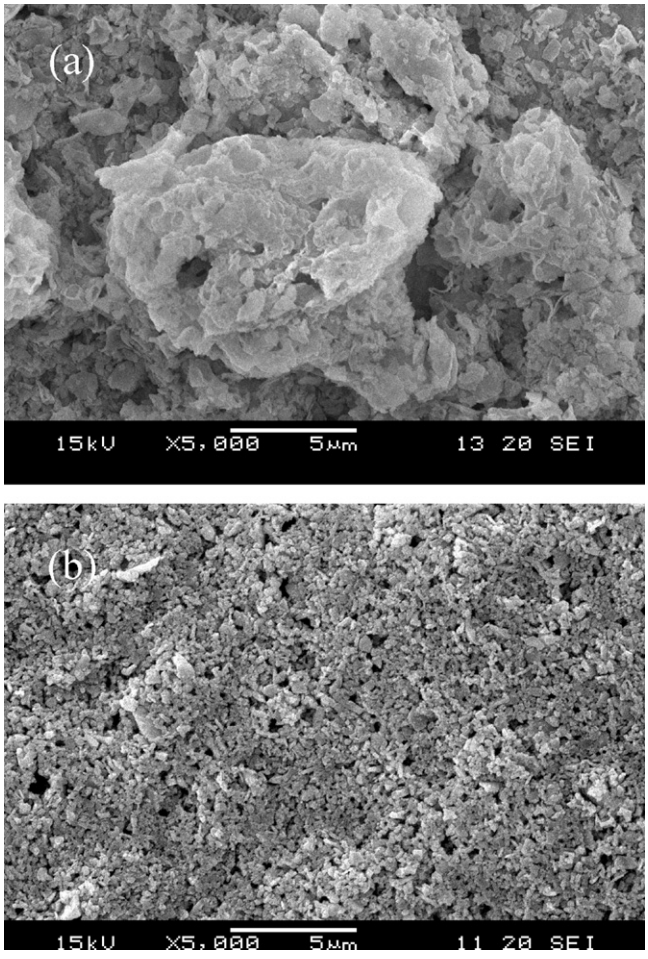

Fig. 8. SEM images of the auto-combustion products (a) and the powders annealed at 800 °C for 2 h (b).

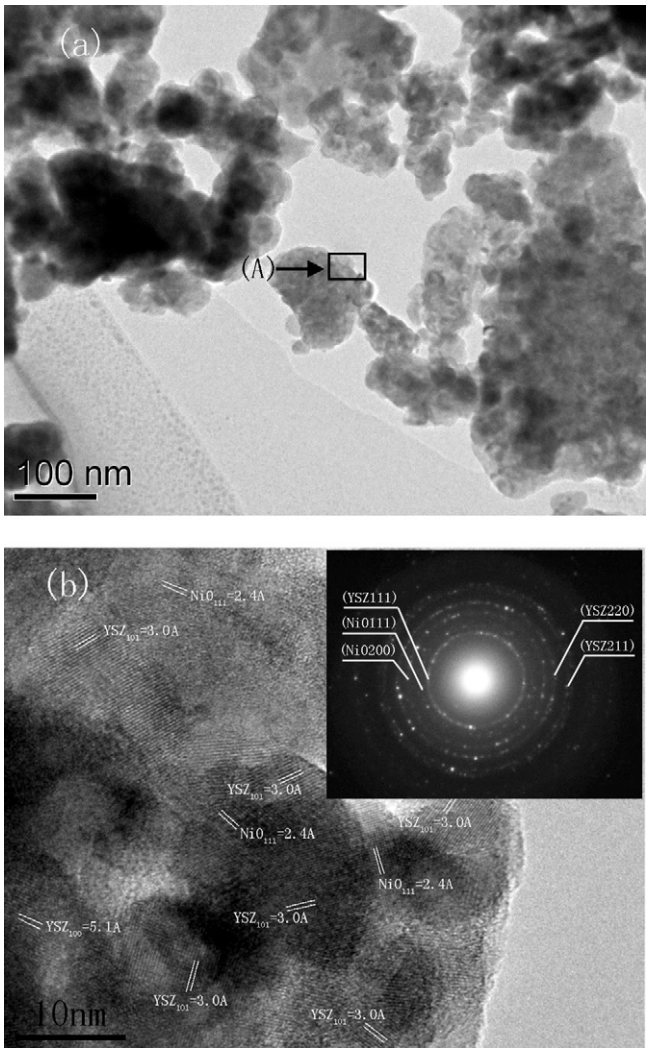

Fig. 9. TEM image of the combustion product after annealing at 800 °C for 2 h (a) and HRTEM image of the same (b), with the inset showing the SAED pattern on the spot A in (a).

the one for the samples after annealing at 800 °C for 2 h. From the micrograph (a), it can be seen that the fresh combustion product of the gels is microscopically characterized with fluffy aggregates with a dimension of 5–10 μm. Clearly, such a foamy microstructural feature should be formed by the bursting release of hot gas during the fierce combustion of gels. In contrast, the samples by annealing the combustion products at 800 °C, as shown in Fig. 8(b), are found to have a loosely compacted microstructure built up of tiny particles, whose dimension is approximately 200 nm on average, about 10 times that of the NiO and YSZ crystallites by XRD analysis. It is postulated that these particles should be composed of finer NiO and YSZ grains.

In order to disclose the fine structural details of the particles, analyses by HRTEM and SAED were performed on the particles with the results shown in Fig. 9. The micrograph (a) in Fig. 9 is a typical TEM image of the particles, clearly manifesting the presence of a sub-structure within the particles. A HRTEM image taken on the spot A of the same sample, as shown in Fig. 9(b), demonstrates many sets of lattice fringes with different orientations and interplanar spaces. They each cover an area of about 10–15 nm across on average and are closely coalesced in space without clear boundaries between them. According to the magnitudes of interplanar spaces and the selected area diffraction data, moreover, these lattice images can be well attributed to the NiO and YSZ crystallites, as indicated by the micrograph (b) and the inset electron diffractionin pattern. Therefore, it can be concluded that each particle in the annealed powder sample is actually a composite body of nanosized NiO and YSZ crystallites. They are joined together to form the particles with an average size of about 200 nm, which are then agglomerated into loose powders. Obviously, when their NiO crystallites are reduced into metal particles, such nanocomposite NiO/YSZ particles are expected to provide a greatly enhanced three-dimensional transport network for electrons and oxide ions through Ni–Ni and YSZ–YSZ grain-links as well as tremendous triple-phase boundaries (TPBs) on the particle's surface.

As the experimental supports to the above deducting statements, Figs. 10 and 11 demonstrate the typical AC impedance spectra for the sintered disc anodes prepared by the nanocomposte NiO–YSZ powder obtained by auto-combustion of complex-gels and by the normal powders (~2.5 μm) synthesized via solid reactions, respectively, as well as their Arrhenius plots of oxide ion conductivities versus temperature over the whole temperature range from 550 °C to 800 °C. It can be evidently noted that the total oxide ion conductivities for the nanocomposite-structured anodes are about 35% higher than the ones by normal powders at each temperature from 550 °C to 800 °C. Furthermore, the acti-

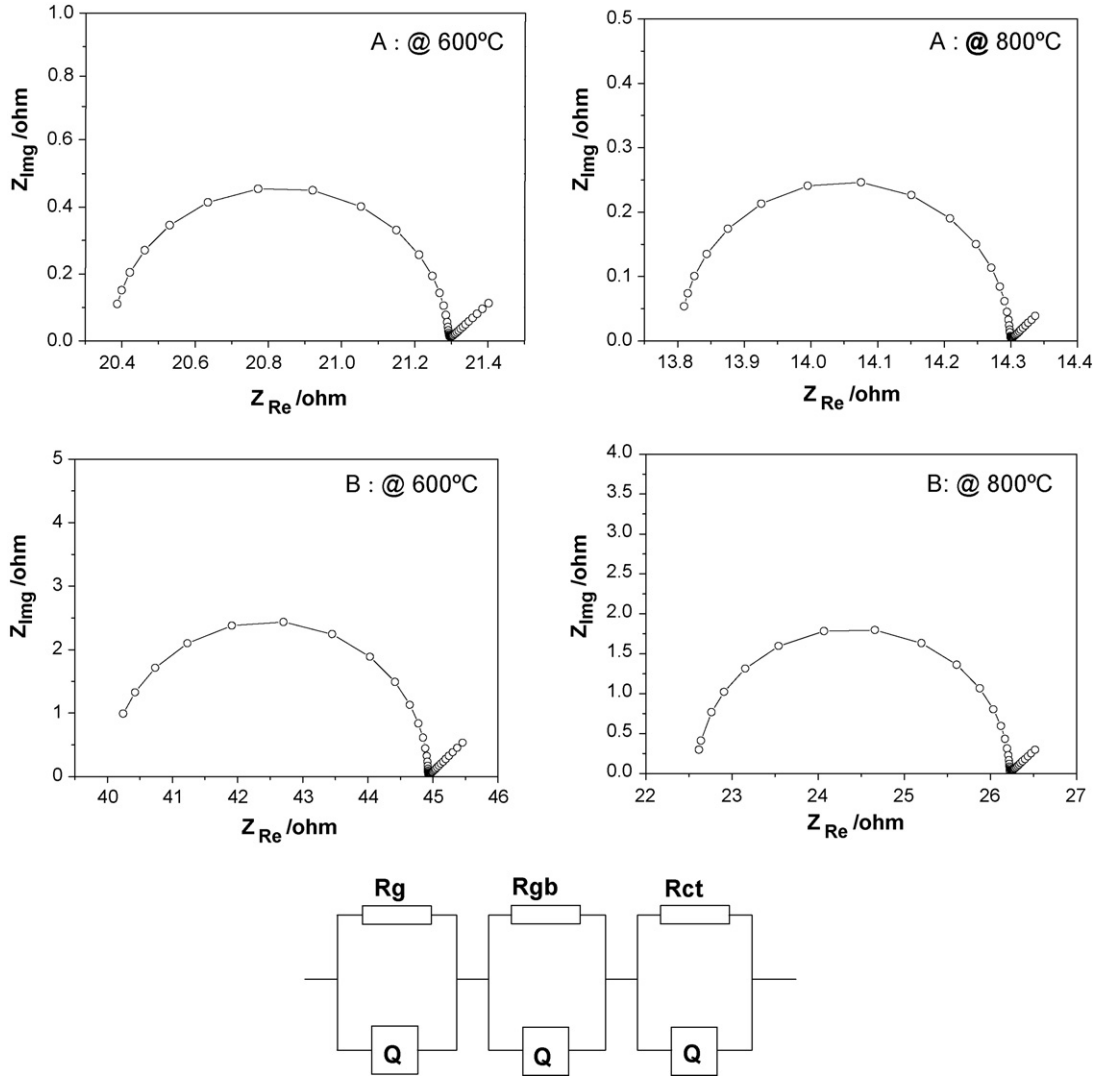

Fig. 10. The exemplified AC impedance spectra at 600 °C and 800 °C for the sintered disc anodes: (A) by nanocomposite powders and (B) by normal powders (~2.5 μm), and the equivalent circuit for data-fitting.

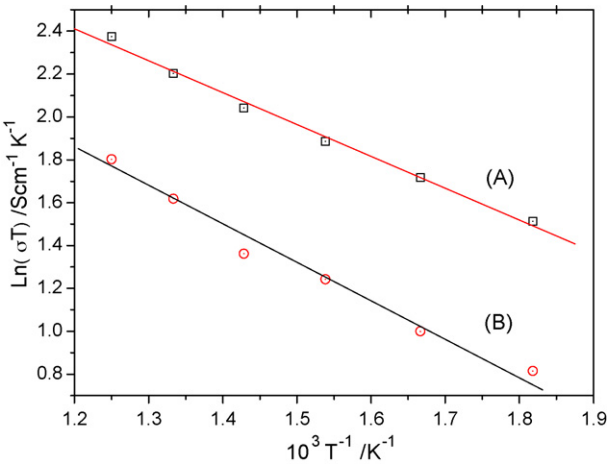

Fig. 11. Arrhenius plots of the conductivities versus temperature for the sintered disc anodes: (A) by nanocomposite powders, and (B) by normal powders (~2.5 μm).

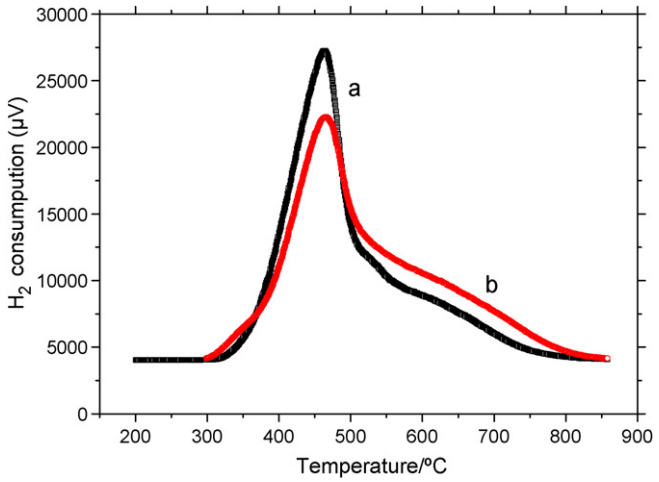

Fig. 12. Temperature programmed reduction curves for the sintered disc anodes (A) by nanocomposite powders and (B) by normal powders (~2.5 μm)

vation energy Ea for these two kinds of anodes can be estimated as 12.30 kJ mol^{-1} and 14.50 kJ mol^{-1}, respectively, according the slopes in their Arrhenius plots in Fig. 11. The smaller value of Ea for the nanocomposite anodes strongly suggests, on the one hand, that the amount of YSZ grain boundary phase contained in these anodes should be much larger than that in the anodes by normal powders because the grain boundary phase of polycrystalline YSZ usually has much lower activation energy than the bulk phase. On the other hand, as shown in Table 4, the grain boundary resistances Rg determined by the semicircle's diameters in AC impedance spectra for these two kinds of anodes at different temperatures indicate that much lower grain boundary resistance Rg is involved in the anodes by the nanocomposite powder than in the ones by the normal NiO/YSZ powder. Moreover, the former appears to be decreased as the temperature increases while the latter changes a little regardless of somewhat erroneous increments. This result means that in the nanocomposite anodes, the grain boundary phase not only has higher volume fraction but also owns lower activation energy than the ones by the normal powders.

As shown in Fig. 12, the temperature programmed reduction (TPR) curves for the two kinds of anodes also give an insight from another angle into the differences between the anodes in microstructures and properties. It can be seen that the nanocomposite NiO/YSZ anodes show a higher and narrower H_2 consumption peak arising around 350 °C than the ones by normal powders, and a lower tailing profile following the peak. Such TPR behaviors clearly indicate that the NiO particles in the sintered NiO/YSZ anodes by the nanocomposite powder should be very small in diameter and narrow in size distribution, as compared with the ones by normal powders, which creates a large volume fraction of surface or interfacial phase and, consequently, leads to a rapid reduction of NiO particle in H_2 when the temperature is raised to 350 °C. It may be better understood if the peaking part of TPR curve is attributed to the reduction of surface and interfacial phase of NiO particles while the tailing part is contributed from the bulk phase made of the cores of NiO particles, whose H_2-reduction should take longer time due to the diffusion of H_2O molecules from the inside of NiO particles. Therefore, it can be concluded that the nanocomposite NiO/YSZ powders can be used to prepare high performance anodes for SOFCs, whose oxide ion conductivity is much higher than the ones made of normal NiO/YSZ powders due to the establishment of a highly dense and well-developed 3D transport network for oxide ions and tremendous triple-phase boundaries (TPBs) on the particle's surface exposed to the pores. Obviously, in the nanocomposite NiO/YSZ anodes, the same scenario will necessarily happen to the electronic conductivity when the NiO particles are reduced.

Table 4
The grain boundary resistance Rg for the anodes by nanocomposite powder and by normal powder.

Temperature (°C)	Grain boundary resistance Rg (Ohm)	
	Nanocomposite powder	Normal powder
550	1.32	3.5
600	1.23	3.6
650	1.11	3.3
700	0.99	3.3
750	0.78	3.7
800	0.51	3.7

5. Conclusions

According to the above experimental results and the analyses thereof, the following main conclusions may be drawn out:

1. With the optimized conditions of CA/M ratio of 1.5 and the pH = 7 based on the quantitative analysis of complexing of metal ions in the aqueous sol, the cations Ni^{2+}, Y^{3+} and Zr^{4+} can be well chelated into the CA-based gel network and then homogeneously dispersed in the dried gels with the desired stoichiometry.
2. The microwave-assisted complex-gel auto-combustion approach with water-soluble nitrates, citric acid and ethyl glycol as starting materials can be effectively employed to prepare highly homogeneous nanocomposite NiO–YSZ powders.
3. By virtue of the short-time, homogeneous *in situ* auto-combustion reactions within the gels, the freshly formed NiO and YSZ crystallites are of almost the same sizes around 14 nm, mainly determined by their relative contents regardless of their crystallization behaviors.
4. The annealing treatment of the combustion products at 600 °C and 800 °C may lead to the coalescence of NiO and YSZ crystallites with an average size of about 15 nm, regardless of a slight grain growth, and the formation of nanoscale composite particles with a size of 200 nm on average, which then tend to loosely and stochastically agglomerate into the powders.
5. The anodes prepared with such nanoscale composite powders have been manifested to possess a larger amount of interfacial phase, lower activation energy Ea for oxide ions transport

and remarkably higher oxide ion conductivity than the ones obtained by normal NiO/YSZ powder (~2.5 μm). Therefore, the nanocomposite NiO/YSZ powders can be used to prepare high performance anodes for SOFCs, which possess a highly enhanced and well-developed 3D transport network for oxide ions and electrons when the NiO particles are reduced, as well as tremendous triple-phase boundaries (TPBs) on the particle's surface promoting the electrochemical reactions.

Acknowledgements

The authors would like to gratefully acknowledge the supports by the Provincial Bureau of Science and Technology, Jiangsu (Grant: BK2006182).

References

[1] T. Razpotnik, M. Marinšek, B. Novosel, K. Zupan, V. Francetič, J. Maček, Ceram. Int. 34 (2008) 1741–1746.
[2] C. Song, Catal. Today 77 (1–2) (2002) 17–49.
[3] S.C. Singhal, K. Kendall, High Temperature Solid Oxide Fuel Cells: Fundamentals Design and Applications, Elsevier Corporation, Oxford, New York, Tokyo, 2003.
[4] Nguyen Q. Minh, J. Am. Ceram. Soc. 76 (3) (1993) 563–588.
[5] H.J. Cho, M.C. Gyeong, J. Power Sources 176 (2008) 96–101.
[6] X. Qi, J. Zhou, Z. Yue, Z. Gui, L. Li, Mater. Chem. Phys. 78 (2002) 25–29.
[7] G.-Q. Shao, H. Cai, J.-R. Xie, X.-L. Duan, B.-L. Wu, R.-Z. Yuan, J.-K. Guo, Mater. Lett. 57 (2003) 3287–3290.
[8] F.-Y. Shih, K.-Z. Fung, H.-C. Lin, G.-J. Chen, J. Power Sources 160 (2006) 148–154.
[9] H. Mohebbi, T. Ebadzadeh, F.A. Hesari, J. Power Sources 178 (2008) 64–68.
[10] A.E. Martell, R.M. Smith, Critical Stability Constants, vol. 3, Plenum Press, New York, 1977.
[11] N.C. Li, A. Lindenbaum, J.M. White, J. Inorg. Nucl. Chem. 12 (1959) 122–128.
[12] Department of Metals, Sun Yat-sen University, Physics and Chemistry Data of Rare Earths, Beijing Metallurgy Industry Press, 1978.
[13] J.-H. Choy, Y.-S. Han, J. Mater. Chem. 7 (9) (1997) 1815–1820.
[14] Z. Jun, C. Jun, Y.-W. Zeng, C.-A. Tian, J. Mater. Sci. Eng. 24 (5) (2006) 737–740.
[15] Y.S. Hong, C.M. Ho, H.Y. Hsu, C.T. Liu, J. Magn. Magn. Mater. 279 (2004) 401–410.
[16] S. Yan, W. Ling, E. Zhou, J. Cryst. Growth 273 (2004) 226–233.
[17] W.-D. Yang, Y.-H. Chang, S.-H. Huang, J. Eur. Ceram. Soc. 25 (2005) 3611–3618.
[18] M. Matzapetakis, C.P. Raptopoulou, A. Terzis, A. Lakatos, et al., Inorg. Chem. 38 (4) (1999) 618–619.
[19] J. Liu, X. Fei, X. Yu, Z. Tao, L. Yang, S. Yang, J. Non-Cryst. Solids 353 (2007) 4697–4701.
[20] S. Musić, S. Popović, S. Dalipi, J. Mater. Sci. 28 (1993) 1793–1798.
[21] F. del Monte, W. Larsen, J.D. Mackenzie, J. Am. Ceram. Soc. 83 (3) (2000) 628–634.